Title

Comparison of Pseudo-Static Limit Equilibrium and Elastic Wave Equation Analyses of Dynamic Earth Pressures on Retaining Structures

Journal

GEOTECHNICAL EARTHQUAKE ENGINEERING AND SOIL DYNAMICS V: NUMERICAL MODELING AND SOIL STRUCTURE INTERACTION, 2018-June(292)

ISSN

0895-0563

Authors

Wagner, Nathaniel
Sitar, Nicholas

Publication Date

2018-06-07

DOI

10.1061/9780784481479.035

Peer reviewed

Comparison of Pseudo-Static Limit Equilibrium and Elastic Wave Equation Analyses of Dynamic Earth Pressures on Retaining Structures

Nathaniel Wagner, Ph.D., P.E., M.ASCE[1]; and Nicholas Sitar, Ph.D., P.Eng., M.ASCE[2]

[1]SAGE Engineers, Inc., Oakland, CA 94612. E-mail: nwagner@sageengineers.com
[2]Edward G. Cahill and John R. Cahill Professor, Dept. of Civil and Environmental Engineering, Univ. of California, Berkeley, CA 94720-1710. E-mail: sitar@berkeley.edu

ABSTRACT

The seismic earth pressure increment is typically computed using either pseudo-static limit equilibrium methods or elastic wave equation analyses of the interaction between a retaining structure and backfill material, yet current interpretations of the two methods provide conflicting recommendations. The focus of this study is to compare the seismic earth pressure increment computed using the two methods. This approach is demonstrated by subjecting an initially uniform prototype site selected from standard site classifications to harmonic excitation in one-dimensional equivalent linear analyses. Then, the seismic earth pressure resultant for a rigid wall is computed using the two methods. The limit equilibrium approach utilizes the acceleration records from the equivalent linear analysis to compute a seismic coefficient, whereas the elastic solution incorporates the reduced modulus and damping from the final iteration of the analysis, as well as the relative displacement records. The results presented herein corroborate the findings of recent centrifuge experiments and associated analyses.

INTRODUCTION

Analytic and semi-analytic approaches to computing seismic earth pressures on retaining structures typically use either pseudo-static limit equilibrium solutions (e.g., the Mononobe-Okabe method) and/or elastic wave equation analyses. The two approaches seem to provide different results and recommendations when compared to one another; i.e., the seismic earth pressure increment is lower for limit equilibrium methods and higher for elastic methods, in general (see e.g. Brandenberg et al., 2015). Recent experimental results (Sitar et al., 2010; Candia et al., 2016; Mikola et al., 2016) demonstrate that the limit equilibrium solutions over predict observations when the surface PGA is used as the input acceleration, as is commonly recommended. Additionally, Wagner and Sitar (2016) demonstrate that limit equilibrium solutions more closely agree with experimental results when the effect of incoherence is accounted for in the input acceleration. However, while simpler to use and in good agreement with experimental results, pseudo-static limit equilibrium methods do not lend themselves to analysis of layered profiles of soils with varying properties, nor do they explicitly include the flexibility of the wall; whereas elastic methods can more readily account for such settings. In this paper we present an example analysis using a single soil profile with consistent properties subjected to harmonic excitation in order to compare the two different approaches. In particular, we attempt to show the difference in magnitude of the resulting dynamic loads based on the method of analysis and how they compare to recent experimental results. The goal is to demonstrate that recommended analysis procedures can produce unrealistic and confusing results if they are not carefully applied.

spaceMETHODS OF ANALYSIS

Pseudo-Static Limit Equilibrium

The classic pseudo-static limit equilibrium procedure is based on the work of Okabe (1924) and Mononobe and Matsuo (1929), and it is collectively known as the Mononobe-Okabe (M-O) method. More recent extensions and modifications of the M-O method (e.g., Mylonakis et al., 2007; Shukla et al., 2009; Iskander et al., 2013) are based on a similar set of assumptions and provide comparable results. The most difficult task in applying the M-O method is in the selection of the horizontal seismic coefficient, k_h. Accepted design standards typically recommend using the PGA or some fraction thereof (e.g., Anderson et al., 2008). The main limitation of the method is the assumption of a rigid wedge developing behind the wall, implying an infinite shear wave velocity and a discrete failure surface. Steedman and Zeng (1990) applied a sinusoidal acceleration profile to the backfill assuming a non-infinite shear wave velocity and concluded that the phase change of the inertial demands within the wedge did not have a significant effect on the total seismic load. The solution, however, neglects energy dissipation in the soil and violates the boundary condition of zero shear stress at the surface; as a result the seismic load decreases monotonically with increasing frequency, contrary to expected dynamic soil response. Candia et al. (2014) developed a hybrid solution based on elastic wave propagation in the backfill that correctly accounts for the boundary conditions and energy dissipation in the soil and obtained a good match with experimental results. However, this approach is not based purely on elastic wave propagation, as it uses limit equilibrium to solve for the resultant, thus inheriting some of the limitations of the M-O method.

Linear Elastic Wave Equation Analysis

Linear elastic closed form solutions have been proposed by a number of investigators, including Veletsos and Younan (1994a/b, 1997) and Younan and Veletsos (2000), and more recently Brandenberg et al. (2015, 2017). These methods offer an alternative to the limit equilibrium methods and have the advantage that they can consider elastic wave propagation and the relative motion between the soil and the structure, and provide rigorous solutions that can be tested against experimental results. In fact, Brandenberg et al. (2015) analyzed the results of centrifuge experiments by Al Atik and Sitar (2010) and showed that the results match reasonably well with the kinematic framework in terms of the magnitude of the seismic earth pressure resultant; however, their results do not match the seismic earth pressure distribution observed in the centrifuge experiments. Following Veletsos and Younan (1997), it seems that the missing factor is the inclusion of realistic wall flexibility (Figure 1a), characterized by $d_w = GH^3/D_w$ where G is the secant elastic shear modulus of the backfill, H is the backfill height, and $D_w = E_w t_w^3/12\left(1-\nu_w^2\right)$ is the flexural rigidity per unit length of wall, which substantially lowers the dynamic pressure compared to the rigid wall case ($d_w = 0$). The base flexibility, characterized by $d_\theta = GH^2/R_\theta$, where R_θ is the torsional spring constant, provides a modest decrease in dynamic pressure compared to walls rigidly constrained at the base ($d_\theta = 0$), as shown in Figure 1b. Including wall and base flexibility shows that the pressure distribution becomes roughly triangular with depth and the point of force application decreases from 0.6 H for a rigid wall to less than 0.3 H for a flexible cantilever wall, as shown in Figure 1c. Veletsos

spaceand Younan (1997) conclude that including realistic wall and base flexibility leads to a significant reduction in seismic forces and the effective resultant can be applied at 1/3 H, a conclusion that was also arrived at by Mononobe and Matuso (1932).

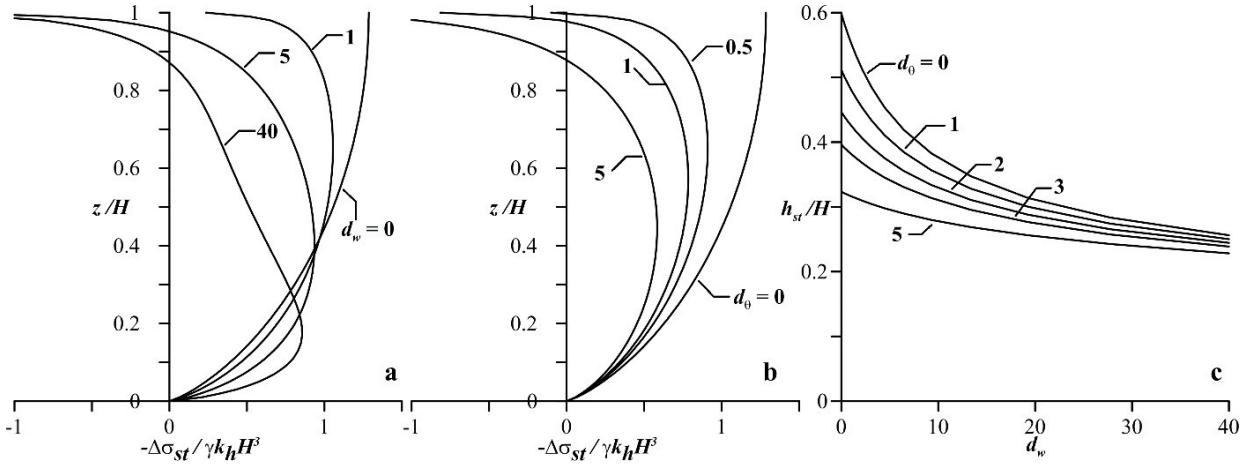

Figure 1: a) Normalized wall pressure as a function of increasing wall flexibility (dw); b) normalized wall pressure as a function of increasing rotational flexibility (d_θ) c) location of the point of force application as a function of wall flexibility for cantilever walls. Reproduced following Younan and Veletsos (1997)

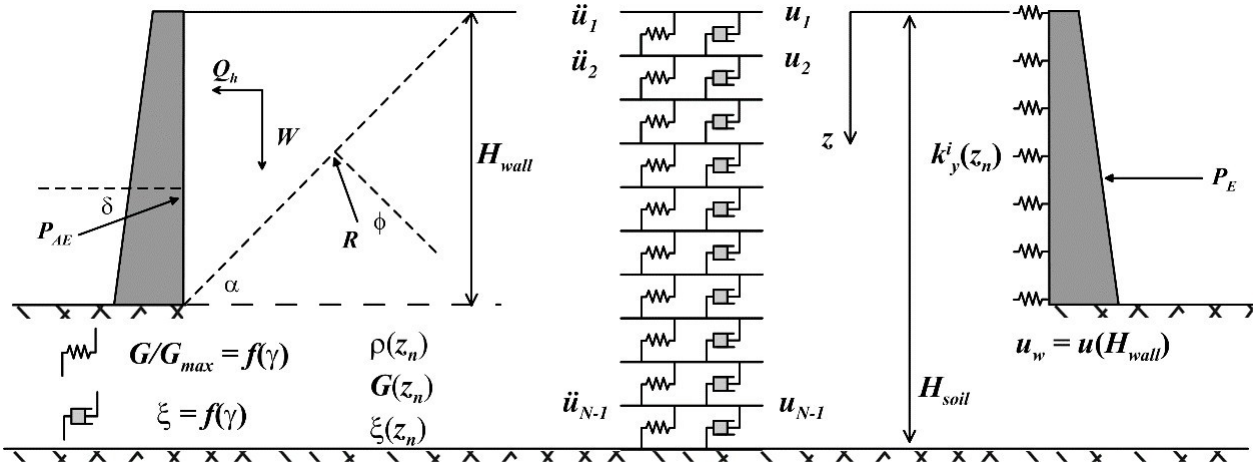

Figure 2: Alternative approaches to analysis of seismic earth pressures on rigid walls: Limit equilibrium method with finite shear wave velocity (left), equivalent linear viscoelastic wave equation analysis (right).

COMPARITIVE ANALYSIS

To illustrate the difference between the two approaches we analyzed two different cases using the same site conditions as shown in Figure 2. The site is modeled as a 1D soil column representing the free field, from which equivalent linear viscoelastic properties, acceleration and displacements are obtained. The left side of Figure 2 shows a rigid wall on a viscoelastic foundation with the soil acting on the wall as a Coulomb wedge. The alternative model, shown on the right side of Figure 2 is a rigid wall attached at its base to a viscoelastic foundation and connected to the 1D column through a series of frequency-dependent, equivalent Winkler spacesprings, similar to that used in Brandenberg et al. (2015). In this case the foundation input motion is equal to the free field motion at the same depth and the wall cannot rotate.

Soil Profile

An initially uniform 30 m deep site on an elastic halfspace is selected to correspond with ASCE 7-16 Site Class D (ASCE, 2017). The unit weight, γ, is 19 kN/m^3, initial shear wave

velocity, V_s , is 270 m/s, and the friction angle, ϕ , is estimated as 35° for the range of average blow counts (N = 15 to 50 bpf) in the site classification. The site is discretized into 100 layers of equal thickness. Modulus reduction, G / G_{max}, and damping curves, ξ , are developed using the Generalized Quadratic/Hyperbolic (GQ/H) model formulated by Groholski et al. (2016). The curves are calibrated to Darendeli (2001) curves in the small strain regime ($\gamma < 0.1\%$) for OCR of 1, PI of 0, *K0* of 0.5, and a target shear stress calculated as τ_{max} σ' $\tan\phi'$ for each layer. The modulus reduction and damping curves are shown in Figure 3. Note that the modulus degradation and damping curves for the top layer, Layer 1, represent a significantly softer soil; the curves for Layer 4 through Layer 101 are more similar to each other, reflecting more similar modulus reduction and damping behavior below the depth of 0.9 m.

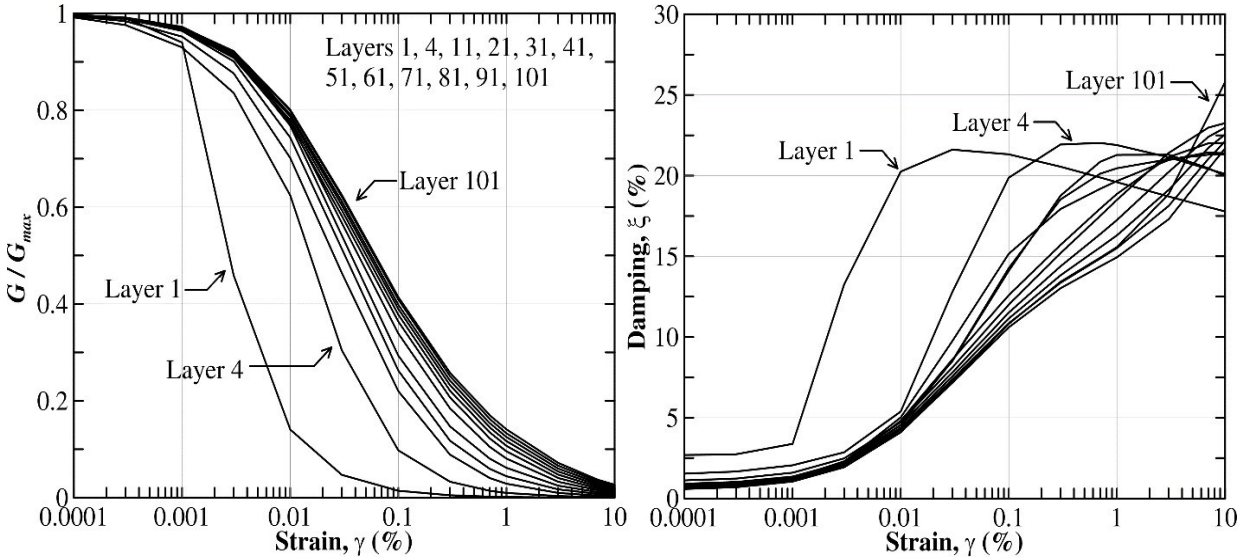

Figure 3: Modulus reduction and damping curves based on GQ/H Model (Groholski et al, 2016) calibrated to small strain range of Darendeli (2001) curves

Harmonic Input Motions

space A suite of 105 harmonic input motions were developed with peak accelerations, a_{max} space, of 0.1 spaceto 0.7 g in increments of 0.1 g and periods, T , of 0.05, 0.075, 0.1, 0.15, 0.2, 0.3, 0.5, 0.75, 0.8, 0.9, 1, 1.5, 2, 3, and 5 seconds. The upper limit of the peak acceleration corresponds to the peak k_h admissible by the M-O method for ϕ = 35°. The input motions are defined by 10 sine wave cycles multiplied by an envelope function to provide a gradual buildup and decay of the wave (Equation (1). The input motions are padded with two periods of zeros at the beginning and end; spacea plot of the input ground motion for a_{max} space= 0.7 g and T = 0.1 seconds is shown in Figure 4.

space

$$\text{space}\ddot{u}\left(\frac{\quad}{\quad}\right) = a_{max}\sin\left(\frac{2\pi t}{\quad}\right)\left(1-\cos\left(\frac{2\pi t}{\quad}\right)\right) \quad (1)$$

space

space$u$ 0, t

space$\|$ T $\|$ $\|$

space 2 10T

σπαχε

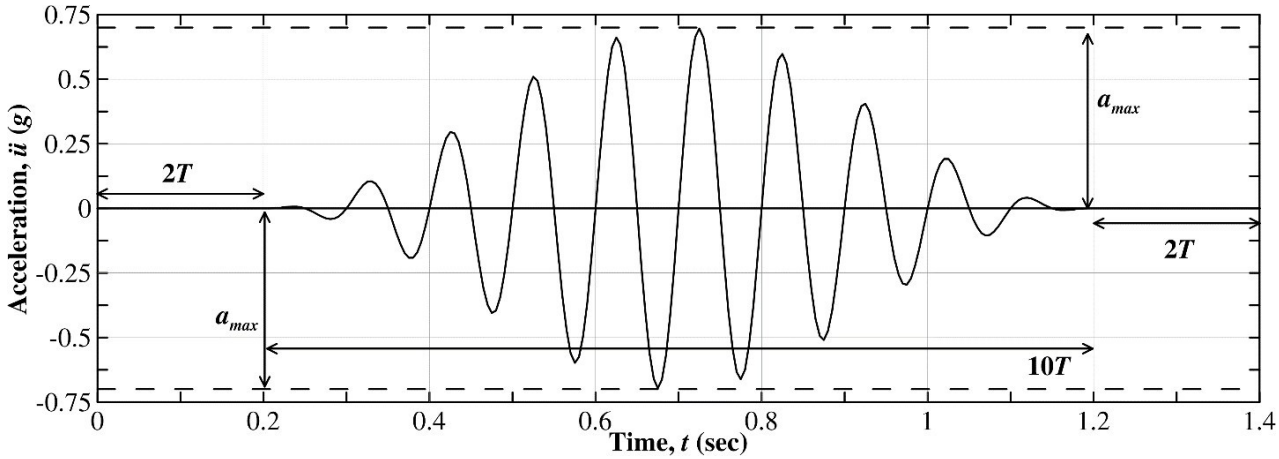

σπαχεFigure 4: Typical input harmonic ground motion (a_{max} space= 0.7 g and T = 0.1 sec)
space

Equivalent Linear Analysis and Seismic Earth Pressure Resultant

The site response is computed using SHAKE (Schnabel et al., 1972), the input motions are applied as an outcropping motion at the top of the soil column in SHAKE, and the motion is deconvolved through the soil profile using a strain ratio of 0.65 for all cases. The acceleration and displacement are recorded at each layer interface, as are the final iterated shear modulus and damping for each layer. The horizontal seismic coefficient for the pseudo-static limit equilibrium method, k_h, is computed by integrating the inertial load in an assumed wedge of the backfill (Equation (2)) and dividing by the weight of the wedge for each of five wall heights, H_{wall}: 3, 6, space9, 12, and 15 m. The maximum value of k_h spaceis used to determine the total seismic earth pressure spacecoefficient, spaceK_{AE} space, using Equation (3)),

space$\left(H - z \right)$ spaceH_{wall}

$$\text{space}Q_h(t) = \int \rho(z) \Big|_{\text{wall}} \Big| u(z,t)dz \Longrightarrow$$

σπαχε

$$\approx \sum_{n=1}^{n=N} \rho(z_n) \Big\lceil \qquad \Big\rceil \qquad 0$$

space$\left(\tan\alpha \right)$

$$\sin\sqrt{\text{?????????}\sin\text{?????????i??}}$$
$$\text{?1?}\cos\sqrt{\text{?????????cos ?i ?????????}}$$
space(2)

$$\text{space}\sum_{n=1} 2\tan\alpha \Big\lfloor (H_{wall} - z_n)u(z_n,t) - (H_{wall} - z_{n-1})u(z_{n-1},t) \Big\rfloor \Delta z_n$$

$$\text{space}K_{AE} = \frac{\text{space}\cos^2(\phi - \theta - \beta)}{\cos\theta\cos^2\beta\cos(\delta + \beta + \theta}$$

space$_2$ (3)

space)

where ϕ is the angle of internal friction of the soil, δ is the angle of wall friction, β is the slope of the wall relative to the vertical, i is the slope of the backfill relative to the horizontal, $\theta = \tan^{-1}\left(k_h / \left(1 - k_v\right)\right)$, k_h is the horizontal seismic coefficient (in g), and k_v is the vertical seismic coefficient (in g). For this analysis, a level backfill, a vertical wall, and no vertical seismic coefficient are assumed ($i = \beta = k_v = 0$). Lastly, the static active earth pressure coefficient, K_A, spaceis subtracted from

spaceK_{AE}

spaceto obtain the dynamic component of the seismic earth pressure

space

spacecoefficient, ΔK_{AE}.

spaceThe kinematic seismic force increment, P_E

space, is computed as in Brandenberg et al. (2015),

spacewith the modification that the imposed free field ground displacements are arbitrary in time (Equation (4)). The horizontal soil-wall reaction stiffness, $k_y^i(z)$, is modified from the original as presented in Kloukinas et al. (2012) to incorporate a non-uniform shear modulus profile (Equation (1)).

$$P = \int_0^{H_{wall}} k_y^i(z)\left[u(z,t) - u_w(z,t)\right] dz \Longrightarrow$$

space

$$\approx \sum_{n=1}^{n=N} k_y^i(z_n)\left[\left(u(z_n,t) - u_w(z_n,t)\right) - \left(u(z_{n-1},t) - u_w(z_{n-1},t)\right)\right] \Delta z_n \quad (4)$$

space

$k_y^i(z) =$

space(5)

spaceNote that the horizontal soil-wall reaction stiffness, k_y

space, from Kloukinas et al. (2012) is

spacemathematically equivalent to that interpreted from Veletsos and Younan (1994a). The dynamic stiffness modifier (the square root on the right-hand side of Equation (1)) is manipulated to use the effective period of the first-mode of vibration of the backfill over the height of the wall,

space$T_{s,H}$

space, since the shear wave velocity is allowed to vary with depth according to the final iterated

spaceequivalent linear properties. Poisson's ratio, ν, is set to 0.3. The normalized kinematic seismic

spaceforce increment,

spaceK_E, is computed by dividing

spaceP_E by

space$\frac{1}{2}\gamma_{wall} H^2$ –

spacefor comparison to ΔK_{AE} from

spacethe pseudo-static limit equilibrium analysis.

RESULTS

The results of the limit equilibrium (ΔK_{ae}
space

) and elastic analyses (K_E
space

) for two different input

spaceperiods (T = 0.1 s and 1.0 s) and

spaceH_{wall} = 6 m are plotted against the horizontal seismic

spacecoefficient (selected to be the depth-averaged acceleration as described in Wagner and Sitar, 2016) in Figure 5. The resultant using the M-O method and the single frequency approach described in Brandenberg et al. (2015) for input frequencies of T = 0.1 s and 1.0 s are shown for reference. For simplicity of presentation, the shear modulus is reduced to 70% of the input G_{max} and the damping is set to 5% to approximate the strain compatible properties for all input amplitudes in the single frequency approach. The displacement is related to the input amplitude

spaceas $u_{g\,0}$

space$= a_{max}$

space$/\left(2\pi / T\right)2$

spacesince the input acceleration is harmonic. A constant horizontal soil-wall

spacereaction stiffness is used as this is a strict application of Brandenberg et al. (2015). Additionally, the results of recent centrifuge experiments on 6 m tall prototype walls (Mikola et al., 2016; Candia et al., 2016) are presented for comparison.

spaceFor the case of T = 0.1 s and $k_h \lesssim$

space0.35, the results of the current limit equilibrium and

spaceelastic analyses agree well with the centrifuge results and the Brandenberg et al. (2015)

spaceapproach. For $k_h \gtrsim$

space0.35 and for the case of T = 1.0 s at all input amplitudes, the results of the

spacecurrent elastic analysis are higher than the limit equilibrium analysis and the Brandenberg et al.

space(2015) approach.. The results are similar for the other input periods considered in this analysis.

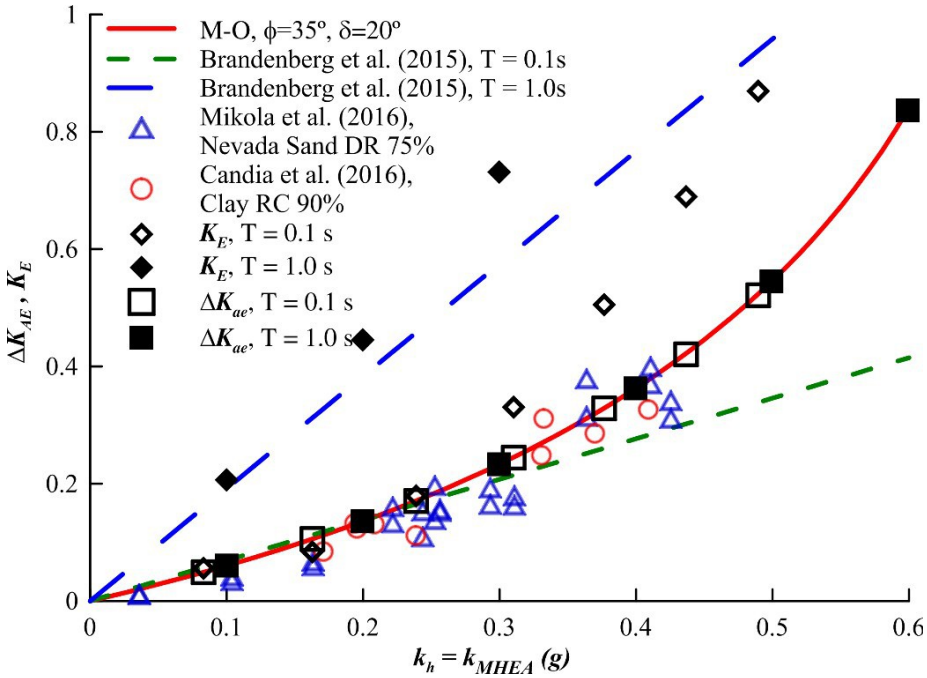

Figure 5: K_E and ΔK_{AE} versus k_h for H_{wall} = 6 m

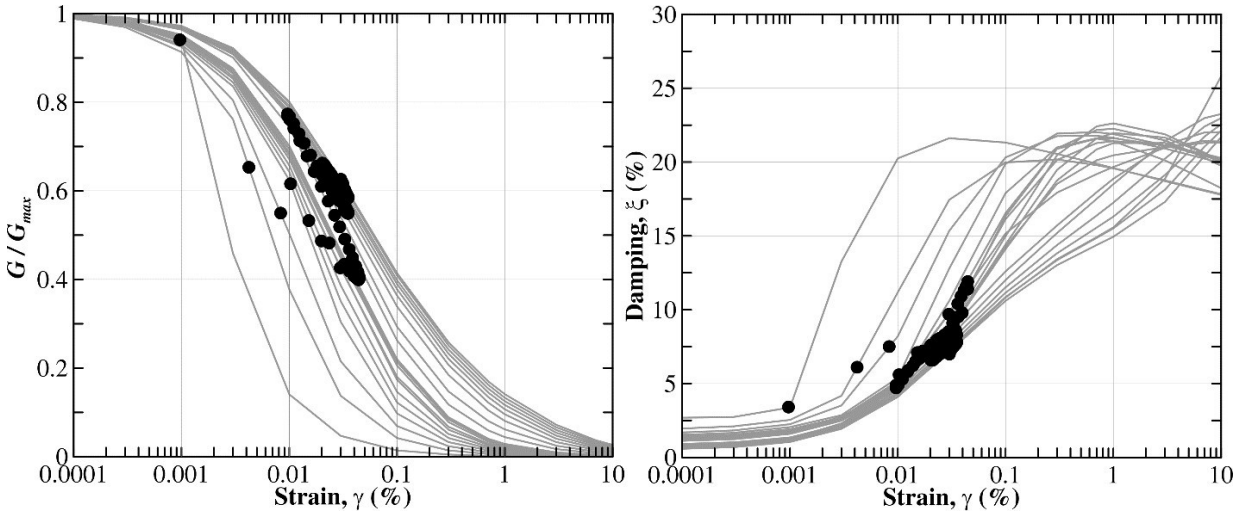

Figure 6: Final iterated modulus reduction and damping for a_{max} = 0.7 g and T = 0.1 sec

The results of the comparison show that the frequency content of the input motion is important to consider when applying the elastic analysis since it is based on the difference in displacement between the wall and the backfill. This effect is magnified in the layers near the surface. The initially uniform shear modulus creates a scenario where the layers near the surface are generally much stiffer than would be expected in reality. The final iterated equivalent linear properties show that the surface zones do not exhibit much internal straining, and instead most of the straining occurs in the mid to deeper layers (Figure 6). Therefore, the computed earth pressure is much larger at the surface than at the base of the wall, as expected based on previous

spaceanalytical results for rigid walls with elastic backfill. This highlights the necessity to include an initially non-uniform maximum shear modulus profile to avoid unrealistic results in elastic analyses.

Note that the final iterated equivalent linear strains are non-zero, but not particularly large. This violates the assumptions of a rigid wedge in the backfill for the M-O method and the assumption of a state of plastic equilibrium throughout the backfill required to achieve an initial active earth pressure condition. The two conditions contradict each other, but the strains in the analysis lie between the levels required to achieve either condition. For the purposes of this study, this result is deemed reasonable since the intent is to use the results from the M-O method as a proxy for "realistic" values based on the conclusions from Wagner and Sitar (2016).

As a different comparison, the results of the limit equilibrium and elastic analyses are directly compared to each other in Figure 7 for various wall heights. Each data point relates the spacevalues of ΔK_{ae} spaceand K_E spaceresulting from the same harmonic input motion with a given input spaceperiod. A solid line designates equal values of ΔK_{ae} spaceand K_E space, and a dashed line designates the spacecase of K_E space= 5 ΔK_{ae} space, for reference.

space

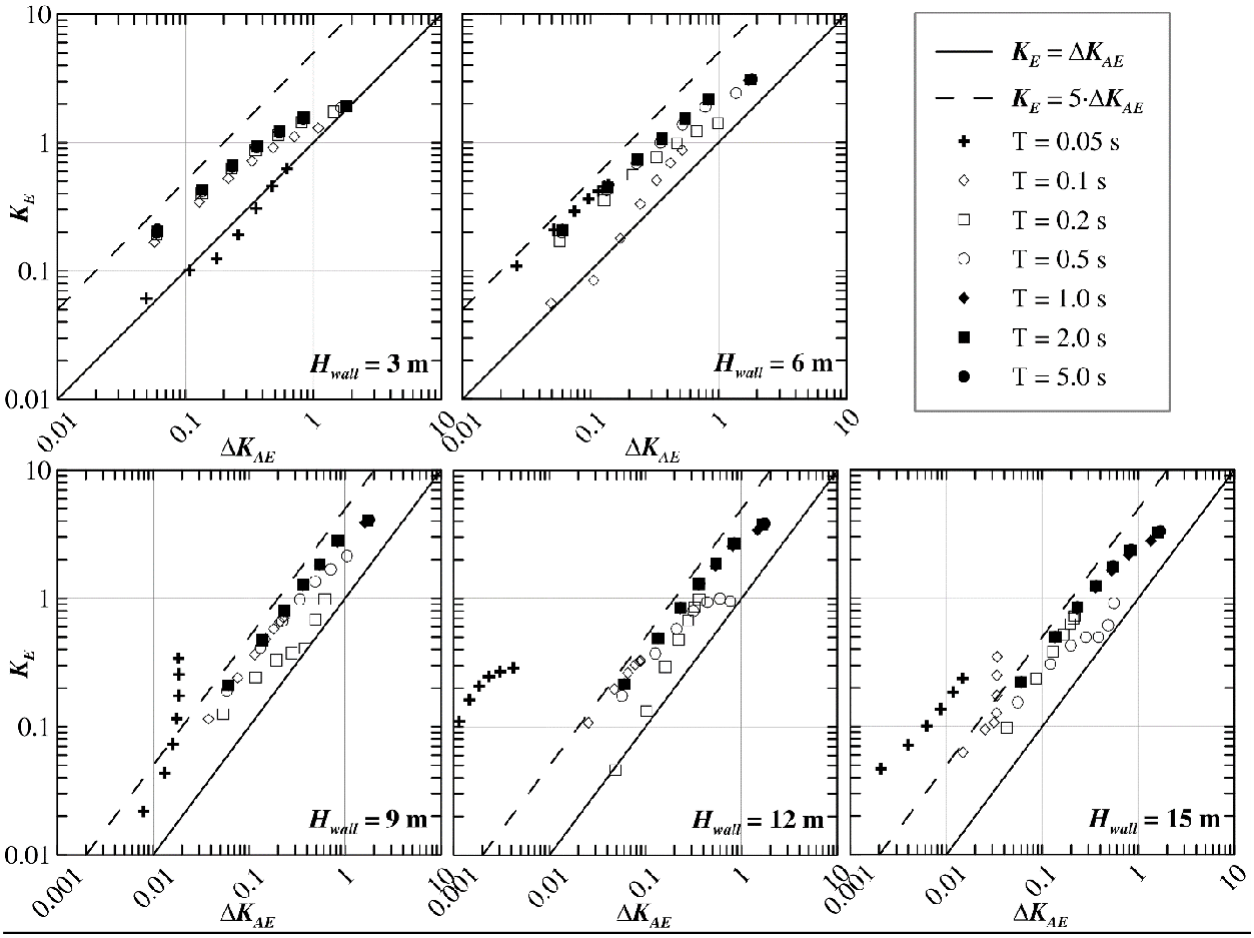

space**Figure 7: K_E space vs ΔK_{AE} space for space H_{wall} space= 3, 6, 9, 12 and 15 m**

space

space For short retaining structures, i.e., space $H_{wall} \lesssim$ space 6 m, K_E space generally exceeds ΔK_{AE} space by a factor of space five at most. The results correspond to the results of Brandenberg et al. (2015), who observed that seismic earth pressure in centrifuge tests by Al Atik and Sitar (2010) are slightly lower than that predicted using their kinematic framework. However, including equivalent linear properties helps to reduce the difference between the limit equilibrium and elastic analyses for short, rigid walls.

space For tall retaining structures, i.e., space $H_{wall} \gtrsim$ space 9 m, K_E space, exceeds ΔK_{AE} space for almost all of the cases that were considered. The most notable finding is that K_E space greatly exceeds ΔK_{AE} space for high frequency input motions because the limit equilibrium solution is affected by the greater incoherence caused by averaging acceleration over the depth, resulting in lower ΔK_{AE}. The elastic analysis is affected by the limited shear modulus reduction in the surface layers, as previously discussed, resulting in higher K_E. For periods in the range of interest for most structures (~0.1–1.0 seconds), the results return to the typical trends observed for short retaining structures: K_E is slightly higher than ΔK_{AE}.

CONCLUSIONS

An example analysis is presented to demonstrate the differences between pseudo-static limit equilibrium and linear elastic wave equation analyses for computing seismic earth pressure on routine retaining structures. As has been shown by Wagner and Sitar (2016), the Mononobe-Okabe method correlates well with experimental results if the incoherence of the ground motion in the backfill is appropriately characterized. Veletsos and Younan (1997) and Brandenberg et al. (2015) provide analytical solutions that are more readily adapted to arbitrary soil profiles, different wall constraints, and input ground motions. Reconciling the good agreement between limit equilibrium analyses and centrifuge experiments with the desire for a more robust framework requires further careful comparative analyses in order to verify that results match observed performance as more complicated analytical models are considered.

ACKNOWLEDGEMENTS

The first author would like to thank SAGE Engineers for providing the opportunity to pursue this research and for providing access to computing resources.

REFERENCES

Al Atik, L, Sitar N. (2010). “Seismic earth pressures on cantilever retaining structures.” *Journal of Geotechnical and Geoenvironmental Engineering*, 136(10), 1324–1333.

American Society of Civil Engineers (2017). “Minimum Design Loads and Associated Criteria for Buildings and Other Structures.” ASCE Standard ASCE/SEI 7-16, ASCE, Reston, VA.

Anderson, D.G., Martin, G.R., Lam, I., Wang, J.N. (2008). “Seismic Analysis and Design of Retaining walls, Buried Structures, Slopes, and Embankments.” NCHRP Report 611, Transportation Research Board, Washington, DC.

Brandenberg, S.J., Mylonakis, G., Stewart, J.P. (2015). “Kinematic framework for evaluating seismic earth pressures on retaining walls.” *Journal of Geotechnical and Geoenvironmental Engineering*, 141(7).

Brandenberg, S.J., Mylonakis, G., Stewart, J.P. (2017). “Approximate solution for seismic earth pressures on rigid walls retaining inhomogeneous elastic soil.” *Soil Dynamics and Earthquake Engineering*, 97, 468–477.

Candia, G.A., Sanhueza, C., Sitar, N. (2014). “Evaluación del empuje sísmico en muros de spacecontención en base a un perfil de aceleraciones de campo libre.” *VIII Congreso Chileno de Ingeniería Geotécnica*, Santiago, Chile, November 26–29, 2014.

Candia, G.A., Mikola, R.G., Sitar, N. (2016). “Seismic response of retaining walls with cohesive backfill: Centrifuge model studies.” *Soil Dynamics and Earthquake Engineering*, 90 (11), 411–419.

Darendeli, M. (2001). “Development of a new family of normalized modulus reduction and material damping curves.” Doctoral Dissertation, University of Texas, Austin, TX.

Groholski, D.R., Hashash, Y.M.A., Kim, B., Musgrove, M., Harmon, J., Stewart, J.P. (2016). “Simplified Model for Small-Strain Nonlinearity and Strength in 1D Seismic Site Response Analysis.” *Journal of Geotechnical and Geoenvironmental Engineering*, 142(9).

Iskander, M., Chen, Z., Omidvar, M., Guzman, I., Elsherif, O. (2013). “Active static and seismic earth pressure for c-ϕ soils.” *Soils and Foundations*, 53(5), 639–652.

Kloukinas, P., Langousis, M., Mylonakis, G. (2012). "Simple Wave Solution for Seismic Earth Pressures on Nonyielding Walls." *Journal of Geotechnical and Geoenvironmental Engineering*, 138(12), 1514–1529.

Mikola, R.G., Candia, G.A., Sitar, N. (2016). “Seismic Earth Pressures on Retaining Structures and Basement Walls in Cohesionless Soils.” *Journal of Geotechnical and Geoenvironmental Engineering*, 142(10), 04016049 1–9.

Mononobe, N., Matsuo, M. (1929). "On the determination of earth pressures during earthquakes." *Proceedings: World Engineering Congress 9*: 179–187.

Mononobe, N., Matsuo, M. (1932). “Experimental Investigation of Lateral Earth Pressure during Earthquakes.” *Earthquake Research Institute and Research Institute of Public Works, Department of Home Affairs*, Japan.

Mylonakis, G., Kloukinas, P., Papantonopoulos, C. (2007). “An alternative to the Mononobe-Okabe equations for seismic earth pressures.” *Soil Dynamics and Earthquake Engineering*, 27(10), 987–969.

Okabe, S. (1924). "General theory of earth pressure and seismic stability of retaining wall and dam." *Journal of the Japanese Society of Civil Engineers*, 10(6), 1277–1323.

Schnabel, R.B., Lysmer, J., Seed, H.B. (1972). "SHAKE: A Computer Program for Earthquake Response Analysis of Horizontally Layered Sites." UC Berkeley, Earthquake Engineering Research Center, Report No. EERC 72–12.

Shukla, S.J., Gupta, S.K., Sivakugan, N. (2009). “Active earth pressure on retaining wall for c-ϕ soil backfill under seismic loading conditions.” *Journal of Geotechnical and Geoenvironmental Engineering*, 135(5), 690–696.

Sitar, N., Mikola, R.G., Candia, G.A. (2012). “Seismically induced lateral earth pressures on retaining structures and basement walls.” *Proceedings: Geotechnical Engineering State of the Art and Practice, Geocongress*, 335–358.

Steedman, R.S., Zeng, X. (1990). "The influence of phase on the calculation of pseudo-static earth pressure on a retaining wall." *Geotechnique*, 40(1), 103–112.

Veletsos, A.S., Younan, A.H. (1994a). “Dynamic soil pressures on rigid retaining walls.” *Earthquake Engineering and Structural Dynamics*, 23(3), 275–301.

Veletsos, A.S., Younan, A.H. (1994b). “Dynamic modeling response of soil-wall systems.” *Journal of Geotechnical Engineering*, 120(12), 2155–2179.

Veletsos, A.S., Younan, A.H. (1997). “Dynamic Response of Cantilever Retaining Walls.” *Journal of Geotechnical and Geoenvironmental Engineeringl*, 25, 785–793.

Wagner, N., Sitar, N. (2016). “On seismic response of stiff and flexible retaining structures.” *Soil*

space*Dynamics and Earthquake Engineering*, 91, 284–293.

Younan, A.H., Veletsos, A.S. (2000). “Dynamic Response of Flexible Retaining Walls.” *Earthquake Engineering and Structural Dynamics*, 29(12), 1815–1844.

$$\ddot{u}(0,t) = \frac{a_{max}}{2}\sin\left(\frac{2\pi t}{T}\right)\left(1-\cos\left(\frac{2\pi t}{10T}\right)\right)$$

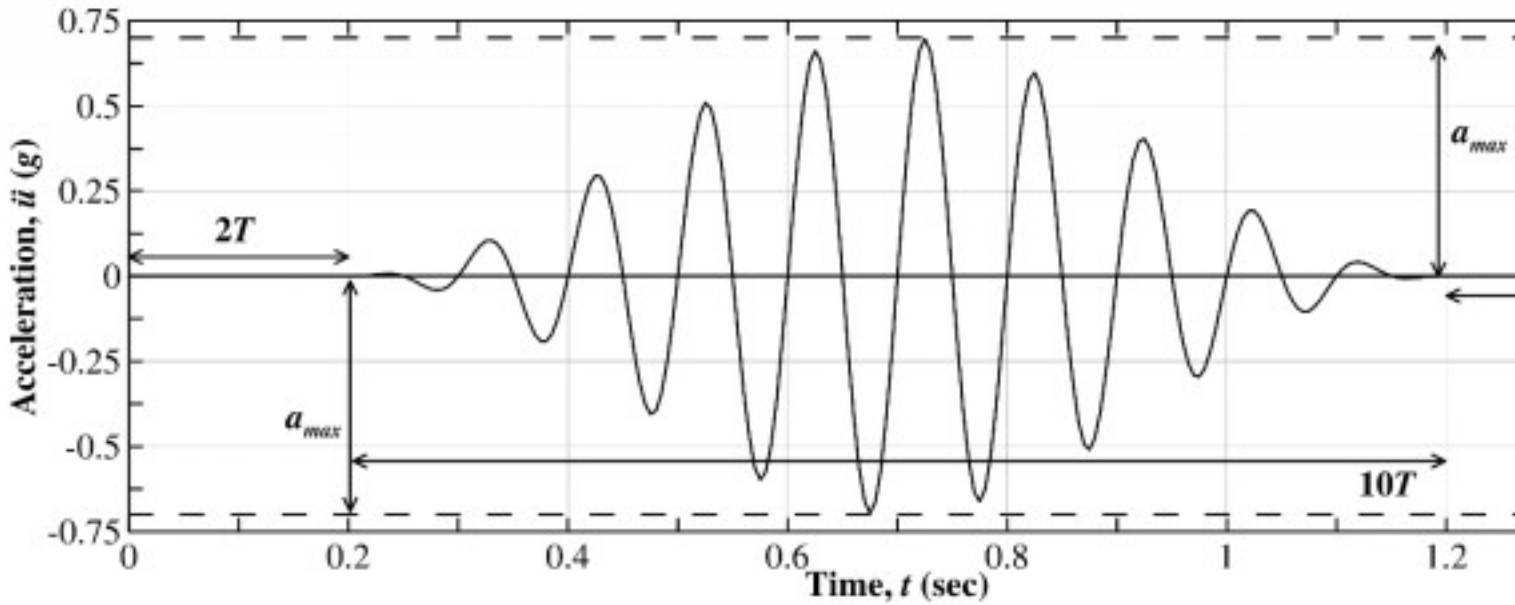

Figure 4: Typical input harmonic ground motion (a_{max} = 0.7 *g* and T = 0.1 se

Equivalent Linear Analysis and Seismic Earth Pressure Resultant

The site response is computed using SHAKE (Schnabel et al., 1972), the input motio applied as an outcropping motion at the top of the soil column in SHAKE, and the motio deconvolved through the soil profile using a strain ratio of 0.65 for all cases. The acceler and displacement are recorded at each layer interface, as are the final iterated shear modu damping for each layer. The horizontal seismic coefficient for the pseudo-static limit equ method, k_h, is computed by integrating the inertial load in an assumed wedge of the back (Equation (2)) and dividing by the weight of the wedge for each of five wall heights, H_{wa} 9, 12, and 15 m. The maximum value of k_h is used to determine the total seismic earth p coefficient, K_{AE}, using Equation (3)),

$$Q_h(t) = \int_0^{H_{wall}} \rho(z)\left(\frac{H_{wall}-z}{\tan\alpha}\right)\ddot{u}(z,t)\,dz \Rightarrow$$

$$\approx \sum_{n=1}^{n=N} \frac{\rho(z_n)}{2\tan\alpha}\left[(H_{wall}-z_n)\ddot{u}(z_n,t)-(H_{wall}-z_{n-1})\ddot{u}(z_{n-1},t)\right]\Delta z_n$$

$$K_{AE} = \frac{\cos^2(\phi-\theta-\beta)}{\left[\sqrt{\quad}\right]^2}$$

$$P_E = \int_0^{H_{wall}} k_y^i(z)\left[u(z,t) - u_w(z,t)\right]dz \Rightarrow$$

$$\approx \sum_{n=1}^{n=N} \frac{k_y^i(z_n)}{2}\left[\left(u(z_n,t) - u_w(z_n,t)\right) - \left(u(z_{n-1},t) - u_w(z_{n-1},t)\right)\right]\Delta z_n$$

$$k_y^i(z) = \frac{\pi}{\sqrt{(1-\nu)(2-\nu)}} \frac{G(z)\sqrt{1+2i\xi(z)}}{H_{wall}} \sqrt{1 - \left(\frac{T_{s,H_{wall}}\sqrt{1+i\xi(z)}}{T}\right)^2}$$